Proceedings of the ASME 2024 Power Conference
POWER2024
September 15-18, 2024, Washington, District of Columbia

POWER2024-138094

IDENTIFICATION OF CONTROL STATE CHANGES IN A POWER PLANT DESUPERHEATER SYSTEM VIA TRANSFER FUNCTIONS AND GAUSSIAN PROCESS MODELING

Claudemi Nascimento[1,†] Victor Alves[1,†], Nor Farida Harun[2,3], Nana Zhou[2,3], Kenneth M. Bryden[4], Lawrence J. Shadle[2], David Tucker[2], Fernando V. Lima[1,*]

[1]Department of Chemical and Biomedical Engineering, West Virginia University, Morgantown, WV, 26506, USA
[2]U.S. Department of Energy, National Energy Technology Laboratory (NETL), Morgantown, WV, 26505, USA
[3]NETL Support Contractor, Morgantown, WV 26505, USA
[4]Ames Laboratory, Ames, IA, 50011, USA

ABSTRACT

This work presents a novel study for identifying alterations in the control states of a desuperheater system based on real closed-loop data from a coal-fired power plant operating under various loads using linear and nonlinear system identification techniques. Specifically, Transfer Functions (TFs) and Gaussian Processes within a Nonlinear AutoRegressive eXogenous model (GP-NARX) are utilized. The desuperheater system comprises two units, north and south, each modeled as a single-input single-output (SISO) system based on spray valve positions and outlet temperatures. To identify changes in the control states using TFs, deviations in the coefficients of three poles and two zeros transfer functions are analyzed. Significant shifts in the control states of the north desuperheater are observed when transitioning from nominal to half and low loads, with deviations of up to four orders of magnitude. Substantial changes in control states are also observed for the south desuperheater when moving from nominal to low load, with a deviation in the coefficients of up to five orders of magnitude, whereas the transition from nominal to half load shows a smaller deviation of up to three orders of magnitude. In the GP-NARX approach, model uncertainties are used to indicate the changes in the control states. The south desuperheater showed a significant uncertainty of up to $8^{\circ}F$ from the nominal to the low load, evidencing a change in the control states. Regarding the north desuperheater, increased uncertainty, up to $6^{\circ}F$, is also observed but in shorter time intervals when compared to the south desuperheater. Ultimately, this work shows that both approaches can be used as a basis for system identification, employing real closed-loop power plant data.

Keywords: System Identification, Desuperheaters, Power Plants, Gaussian Processes, Transfer Functions

[†]Joint first authors
[*]Corresponding author: Fernando.Lima@mail.wvu.edu

1. INTRODUCTION

A boiler system in a coal-fired power plant (see Fig. 1) is mainly composed of a series of superheaters. After passing by the final superheater, the steam generated flows into a high-pressure turbine. The temperature of the superheated steam is firstly controlled by the amount of coal combustion and the water flow rate supplied to the boiler [1, 2]. However, during a transient operation when the generator load changes, controlling the steam temperature at the desired set-point might be difficult due to the inherent nonlinearity of boiler systems. This challenge in controlling the steam temperature may lead to a steam temperature above the set-point, which increases thermal and pressure stresses on the system, thus accelerating component degradation and failure.

To ensure control of the steam temperature, a desuperheater is used to regulate the temperature of the superheated steam between the superheaters, aiming to achieve the desired turbine-inlet temperature during both steady-state and transient operations. A desuperheater consists of a device that sprays water into the superheated steam coming from the boiler system. The desuperheated temperature is monitored to ensure accurate control of the steam temperature through a thermowell installed after the desuperheater outlet and connected to the feedback control system of the spray water. This design ensures the spray water evaporates before reaching the thermowell, maintaining precise temperature control. Nevertheless, due to the tight arrangement of superheaters inside the boiler, this positioning of the temperature sensors is not always possible, which may lead to unevaporated cold droplets impinging on the thermowell [3]. This latter fact results in the temperature reading being lower than the flowing steam's, affecting the steam temperature control. This may also lead to accelerated component degradation and failure, reducing overall plant lifetime, lowering efficiency, and increasing fuel consumption and emissions.

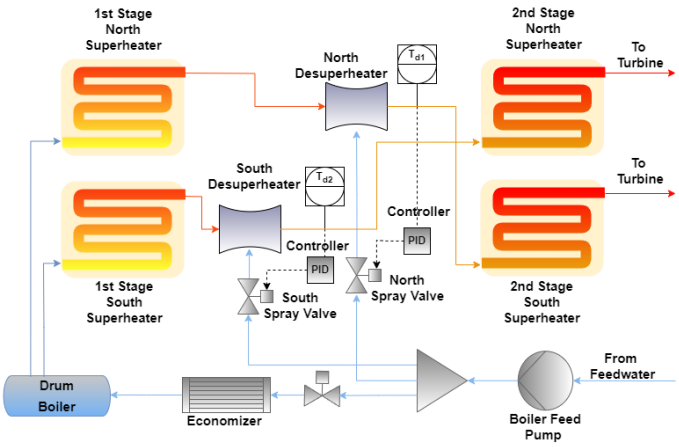

FIGURE 1: Schematic representation of the boiler system with superheaters, desuperheaters, and control elements.

Currently, conventional power plants are challenged to improve operational flexibility and efficiency, especially due to the penetration of renewables into the grid [4]. Identifying ways of improving the operating conditions of these systems while they are fully or partly under closed-loop feedback control brings additional challenges in terms of system identification. While system identification techniques generally work well in open-loop cases, the same is not true for closed-loop cases due to the potential correlations between unmeasured noises and process inputs [5]. Closed-loop system identification techniques have been applied to power plant systems [6]. However, the reported works on closed-loop system identification have not addressed the desuperheater system using both the Transfer Function (TF) and Gaussian Process (GP) approaches. In this work, as a novel contribution, linear and nonlinear system identification using Transfer Functions and Gaussian Processes within a Nonlinear AutoRegressive eXogenous model (GP-NARX) are employed to identify alterations in the control states of a desuperheater system using real closed-loop data from a coal-fired power plant operating at different loads. Abrupt changes in control states can lead to reduced plant lifetime and low efficiency when the power plant is subjected to variations in the loading operating conditions. Real data from a coal-fired power plant in closed-loop at full load (430 MW), 57% load (242 MW) – referred to as "half load" hereinafter, and low load of 20% (82 MW) are used. The proposed approaches can then be used as a basis for system identification, employing real closed-loop power plant data.

The remainder of this work is structured as follows: a summary of system identification is given in section 2 where linear (2.1) and nonlinear (2.2) system identification techniques employed in this work are described; then, the proposed approach using both system identification techniques are detailed in 3, followed by the presentation and discussion of the obtained results in section 4. Lastly, conclusions and suggestions for future research directions are presented in section 5.

2. SYSTEM IDENTIFICATION

System identification involves building mathematical models of dynamic systems based on observed input-output data from the system studied. The identification problem consists of giving a set of input/output past observations to find a relationship to predict future output values. This relationship can be presented as a mapping of the input-output variations from the measured data. The mapping, f, can be linear or nonlinear depending on the nature of the model selected. System identification is an iterative process and has a logical flow following the steps: (i) data collection; (ii) model structure selection and (iii) training; (iv) model validation; and (v) deciding which model will be used, based on performance criteria such as goodness-of-fit, for example. Returning to a previous step is possible at any step in the identification process to improve the quality of the identified model [7]. In this work, two types of mappings for system identification are addressed. Firstly, a linear system identification technique using transfer functions is described in section 2.1. Secondly, a nonlinear system identification approach employing Gaussian Processes is described in section 2.2.

2.1 Linear System Identification

In linear system identification, it is assumed that the system can be represented as a linear model, which implies that the output results from a linear combination of the inputs and the system's internal states. The objective is to find the optimal parameters of the linear system structure selected using input-output data. As an example of a linear system identification method, a transfer function establishes the relationship between two variables within a physical process in the frequency domain (s), in which one variable acts as the cause (input variable, X), while the other serves as the effect (response or output variable, Y) in the frequency domain [8]. The general form of a transfer function is represented in Eqn. 1 below.

$$\mathrm{TF} = G(s) = \frac{Y(s)}{X(s)} \tag{1}$$

Obtaining a transfer function consists of finding a $G(s)$ representing the system dynamic behavior by estimating the coefficients of a given set of regressors in the transfer function model that best represents the input-output relationship. Estimations of the coefficients are performed by applying optimization algorithms that seek to minimize the differences between the responses of the model outputs and the real system outputs. If the physics of the system is already known or can be depicted using governing equations, then $G(s)$ can be derived straightforwardly by converting these governing equations from the time domain to the frequency domain using Laplace transforms. However, when the system's underlying phenomena are not modeled, and/or there is no or limited knowledge about the mathematical relationship between the inputs/outputs, the number of possible transfer functions representing the system can be large. Hence, the TF modeling task becomes selecting which of the possible transfer functions best represents the system behavior.

Transfer functions are usually defined by their number of poles (z_i) and zeros (p_i), and its coefficients (b_m) and (a_m), in which the denominator corresponds to the poles, and the numerator corresponds to the zeros in Eqn. 2. As one can see in this equation, both the denominator and numerator are just linear combinations. It is worth mentioning that although the number

of transfer functions that can represent the dynamic behavior may be large, the number of zeros should not exceed the number of poles, which means that n is always greater than or equal to m ($n \geq m$). The main reason why this constraint is imposed on the TF modeling task is that in a transfer function, poles are associated with the roots of the denominator polynomial, and zeros are associated with the roots of the numerator polynomial [9]. If the number of poles exceeds the number of zeros, this implies that the system response depends on future inputs, thus violating the causality principle [10]. Therefore, selecting a transfer function can become a difficult task for two reasons: first, there is a large number of possible combinations of transfer functions, and trying all of them may become computationally expensive; and second, if the data used to obtain the transfer functions is limited, there is no guarantee that the obtained transfer function represents the true system behavior for other regions not comprehended by the data. These two transfer function characteristics will be better observed in section 3.1.

$$G(s) = \frac{b_m}{a_n} \frac{(s - z_1)(s - z_2)\dots(s - z_m)}{(s - p_1)(s - p_2)\dots(s - p_n)} \tag{2}$$

2.2 Nonlinear System Identification

The general idea behind estimating the coefficients of a given set of regressors for the linear system identification case in section 2.1 is also considered in the nonlinear system identification case. The general nonlinear structure considered is represented in Eqn. 3, where G is some nonlinear function parametrized by θ, and the components of $\varphi(t)$ are the regressors. Nonlinear system identification models can be divided into several groups depending on the choice of the regressors. A few examples are NFIR (Nonlinear Finite Impulse Response), NARX (Nonlinear AutoRegressive eXogenous model), NOE (Nonlinear Output Error), NARMAX (Nonlinear Auto-Regressive Moving Average model with eXogenous inputs), and others. A complete list and description of nonlinear models for system identification can be found in [11].

$$\hat{y}(t \mid \theta) = G(\varphi(t), \theta) \tag{3}$$

The NARX models are of particular interest in this work. NARX models use the input values, $u(k-i)$, and the measured output values, $y(k-i)$, as the regressors. The general structure of a NARX model is presented in Eqn. 4, where n is the maximum lag in the output values, m is the maximum lag in the input values, and ν is white Gaussian noise.

$$\begin{aligned}\hat{y}(k) =& f(y(k-1), y(k-2), \dots, y(k-n), u(k), \\ & u(k-1), \dots, u(k-m)) + \nu\end{aligned} \tag{4}$$

2.2.1 Non-parametric Nonlinear System Identification.

As briefly mentioned above, the general idea behind nonlinear system identification is estimating the coefficients of a given set of regressors where G is some nonlinear function parametrized by θ, and the components of $\varphi(t)$ are the regressors. However, it is also possible to consider G as a non-parametric function. Non-parametric means not assuming a fixed number of regressors to describe the function being modeled. Gaussian Processes are an example of a non-parametric function. For the specific case of the Gaussian Processes, the number of regressors grows with the number of data points. This means that a set of fixed regressors does not define the function, but instead, it is characterized by a mean function (μ) and a covariance function (C_f), as shown in Eqn. 5, that define the relationships between the data points [12–14]. Of particular interest in this work is combining non-parametric functions with nonlinear system identification structures such as the NARX. This combination opens avenues for identifying several different types of dynamic systems with different time scales and degrees of nonlinearity, considering the prediction robustness feature of both nonlinear and non-parametric models.

$$f(\mathbf{x}) \sim \mathcal{GP}(\mu, C_f) \tag{5}$$

2.2.2 NARX models combined with Gaussian Processes (GP-NARX).

The main motivation for employing the GP-NARX technique corresponds to the inherent and readily available uncertainty prediction from GPs as discussed in the literature [12]. A Typical GP-NARX structure consists of using previous input, $u(k-i)$, and measured output, $y(k-i)$, values to obtain output predictions, $\hat{y}(k)$, as shown in Fig. 2. The implementation considered in this work consists of using real plant data, on-site experiments, or stored (historian) data to generate GP-NARX predictors for each desired output for training. By considering the same training data, validation is performed to assess the GP model performance by observing the predicted mean and standard deviation and the absolute error at each time step. Assuming that the model performance is satisfactory, the trained model can then be employed to investigate the system dynamics for data different from the one used for training or to carry out multi-step-ahead predictions for specific cases [13].

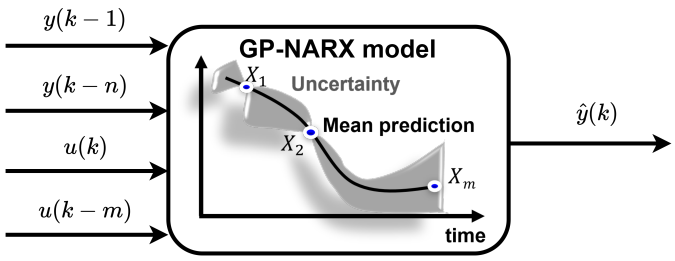

FIGURE 2: Flowchart illustrating the the GP-NARX structure.

3. PROPOSED METHODS

Fundamentally, the methods in this work propose ways of identifying changes in the control states of a desuperheater system in a coal-fired power plant using closed-loop data with the Transfer Function and the GP-NARX schemes. The addressed power plant boiler system is composed of two desuperheaters (north and south) in a power plant with a nominal operating load of 430 MW. A schematic representation of the boiler system containing the two desuperheaters is shown in Fig. 1. The addressed scenario is when operating at loads lower than the nominal, the water spray valve positions traverse the entire range, achieving both

extremes (fully open and fully closed positions) more frequently as the steam pressure and electric load decrease. Consequently, excursions in the desuperheater outlet temperature are observed when the control valve is driven to these extremes. The overall closed-loop control block diagram for the desuperheater system is shown in Fig. 3. The main assumption is that the process (G_p) cannot change by itself without any generated disturbance, noise, or different input values of the manipulated variables (X_V) coming from the actuator (G_v) originated from the controller (G_c). Hence, if the controlled variable ($T_{d,m}$) does not experience a change, the hypothesis is that the control action from (G_c) is not sufficient to move the system to the desired set-points ($T_{d,sp}$), thus causing the excursions in the water spray valve positions.

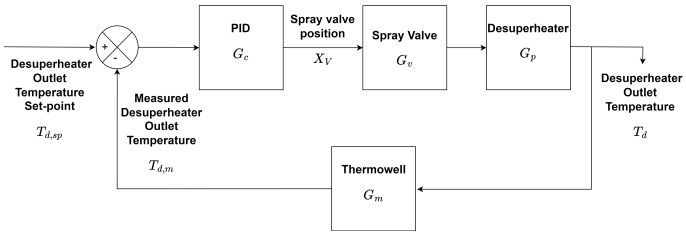

FIGURE 3: Block diagram for the general process control loop.

3.1 System Identification with Transfer Functions

In this approach, alterations in the control states are determined by comparing the model structure (number of poles and zeros) and their coefficients using transfer function identification at multiple operating states. The manipulated variables and controlled variables correspond to valve positions and outlet temperatures of both north and south desuperheaters (see Figs. 1 and 3), respectively, as shown in Tab. 1.

The first step is selecting which transfer function structure best represents the system behavior among the different possible transfer function structures. An automated approach is implemented in MATLAB® using the MATLAB® System Identification™ toolbox to decide on the best structure. The automated approach consists of varying the number of poles and zeros to obtain different transfer function structures and automatically selecting the one that best represents the system behavior, assuming that the system operates at a specified nominal load. The selection of the best transfer function is based on the Goodness-of-fit (GoF) criterion using the Normalized Root Mean Square Error (NRMSE) metric as the objective function. Although the transfer function to be selected is the one that best fits the data, it is important to mention that the main goal is not exclusively model prediction capabilities but also to have a model that is sensible to perform the control state change identification. Therefore, selecting a simpler transfer function structure with a slightly lower accuracy may be better suited to perform identification in the control state change, considering that transfer functions used in control instrumentation are typically of low order [15].

After obtaining the transfer function structure that best fits the system dynamics at the nominal load, the selected TF structure is kept constant with respect to the number of poles and zeros for the remaining load conditions. At this point, system identification at different loads is performed, and the coefficients of the newly identified functions are observed. Deviations are calculated between the coefficients of the newly obtained transfer functions at different loads and the coefficients of the fixed transfer function at the nominal load. The observed deviations are assessed and used as an index to quantitatively identify changes in the control states of the system.

Process	Manipulated Variable	Controlled Variable
North Desuperheater	North Spray Valve Position (X_V^{North}) [%]	Outlet Temperature ($T_{d_1,m}$)[°F]
South Desuperheater	South Spray Valve Position (X_V^{South}) [%]	Outlet Temperature ($T_{d_2,m}$)[°F]

TABLE 1: Manipulated and controlled variables

3.2 System Identification with Nonlinear Auto-Regressive model structure with eXogenous inputs (GP-NARX)

Regarding the GP-NARX approach, the first step consists of training a GP-NARX model based on the data from the system operating at a selected nominal load. For this step, it is necessary to have an appropriate dataset first. Given the inherent form of NARX models, as shown in section 2.2, it is necessary to perform a data table construction based on pre-specified input and output lags. This step means that an additional number of columns, equivalent to the number of lags, are added to both the input and output data. Each column starts and ends at a different point in time following the structure outlined for a GP-NARX problem in Eqn. 4.

After the construction of the appropriate dataset and before performing the training using a GP model, it is necessary to find the initial values of the hyperparameters by computing the log of the marginal likelihood for a given set of hyperparameters and selecting which has the highest likelihood among them. At this step, prior information parameters are provided, such as the bound of hyperparameters, inference method, prior mean function, covariance function, likelihood function, and both input and output data. The specifications on the prior information used in this work are outlined in Tab. 2.

Lastly, the training is performed by informing the selected initial set of hyperparameters and the same prior information parameters used during the initialization procedure. The training consists of the most time-consuming process regarding the use of GP-NARX due to the required inversion of the covariance matrix. After the training step, the optimal hyperparameters are obtained, and the validation of the model against the training data is the next step. Validation assessment can be performed by visually inspecting how the obtained model fits the training data and computing the GoF, for example. After performing validation, the final analysis is carried out to compare how the trained GP-NARX model can represent the system at different loads by assessing the observed model uncertainty. If there is large and extensive model uncertainty, this indicates an alteration in the control states of the system.

Parameter	Value
Hyperparameter bounds	[-4,4]
Inference method	Exact
Mean function	$\mu = 0$
Covariance function	Squared exponential ARD (Eq. 6)
Likelihood function	Gaussian (Eq. 7)

TABLE 2: Informed GP parameters a priory

$$C_f\left(\mathbf{x}_i, \mathbf{x}_j\right) = \sigma_f^2 \exp\left[-\frac{1}{2}\sum_{d=1}^{D} w_d \left(x_{di} - x_{dj}\right)^2\right] \tag{6}$$

$$P = \frac{1}{\left(2\pi\sigma^2\right)^{n/2}} \prod_{i=1}^{n} \left\{\exp\left[-\frac{1}{2}\left(\frac{y^{(i)} - \widehat{f}(\mathbf{x}, \mathbf{w})}{\sigma}\right)^2\right]\epsilon\right\} \tag{7}$$

where w_d and σ_f are the hyperparameters of the covariance function, D is the input dimension, σ is the standard deviation, n is the length of the dataset, y is the output value, $\mathbf{x}$ is the set of input values, $\mathbf{w}$ is the set of parameters, $\widehat{f}$ is the model, and ϵ is the error.

4. RESULTS AND DISCUSSIONS

4.1 System Identification with Transfer Functions

The automated system identification approach for model structure selection outlined in section 3.1 is used to identify which transfer function structure best represents the input-output relationship for both north and south desuperheaters. A specific data set with 322 points sampled each minute at the nominal state (430 MW) is selected as the training set. The number of poles and zeros specified for the transfer function structure selection ranged between one and three, giving six possible combinations, considering that the number of zeros could not exceed the number of poles. The limitation for the range of the number of poles and zeros up to three is imposed, considering that higher-order systems would lead not only to overfitted transfer functions but also excessive computational time for training. The obtained transfer function trends for each desuperheater are shown in Figs. 4 and 5, respectively.

Considering the results for the north desuperheater in Fig. 4, it is possible to visualize that the best transfer function structure corresponds to the one with three poles and two zeros, which has a GoF equal to 47.98%. Other transfer functions evaluated have also exhibited reasonable GoF except for the transfer function with three poles and three zeros, which is shown to be completely off from the true system behavior. Possible reasons for this completely off behavior were not investigated in detail since it would defeat the purpose of this work. However, they are believed to be related to inherent differences in the dynamic nature of the true data and mathematical model characterized by the transfer function. Regarding the results for the south desuperheater in Fig. 5, the transfer function structures with three poles outperform the ones containing one or two poles. Among the ones with three poles, the three poles and two zeros transfer function structure is the one that would best represent the true system behavior with a GoF corresponding to 43.34%. Among all the trained transfer functions, the ones with the highest GoF values are selected to represent the single-input single-output relationship for both the north and south desuperheaters. Therefore, the structures with three poles and two zeros are chosen to represent both north and south desuperheaters for the control states change verification step for the systems at different loads.

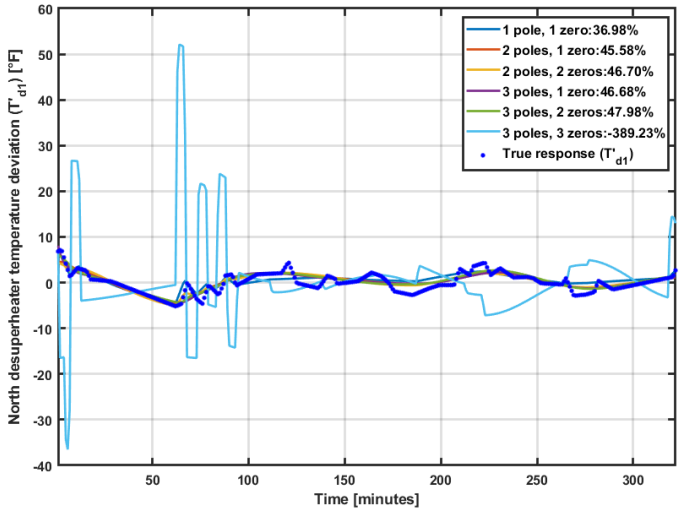

FIGURE 4: High-order transfer functions fitting with accuracy (GoF results) for the north desuperheater.

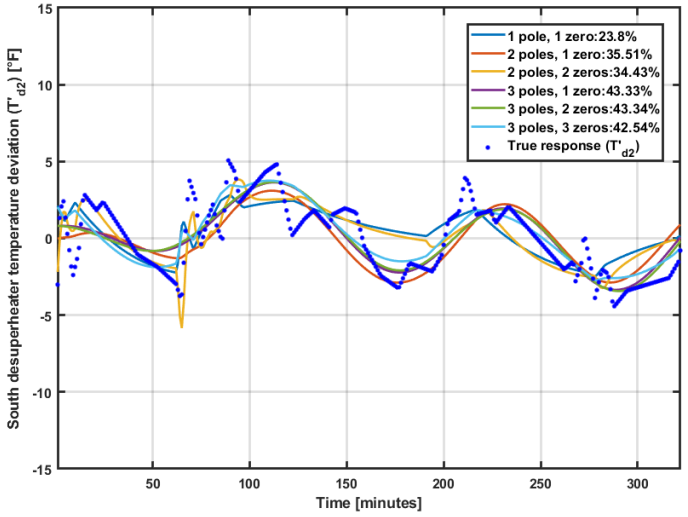

FIGURE 5: High-order transfer functions fitting with accuracy (GoF results) for the south desuperheater.

Before performing the control state change verification, the selected transfer function structures are validated considering the entire system behavior. The parameters of the obtained transfer function structure are fitted again using the entire data with 8,392 points for both north and south desuperheaters. The validations performed are shown in Figs. 6 and 7. The Goodness-of-fit for both north and south desuperheaters for the whole dataset are 48.78% and 30.45%, respectively. Based on the observed GoF

and visually inspecting the trends in Figs. 6 and 7, it is possible to see that in both cases, the transfer functions obtained are able to represent the system behavior at some regions. However, for other parts, the obtained TF structure is not accurate. This latter observation means that a close inspection and analysis of such regions is needed to check if the hypothesis of a possible control state change is indeed happening for the system at different loads, such that the obtained transfer function cannot represent the system anymore whenever a load change happens in the power plant.

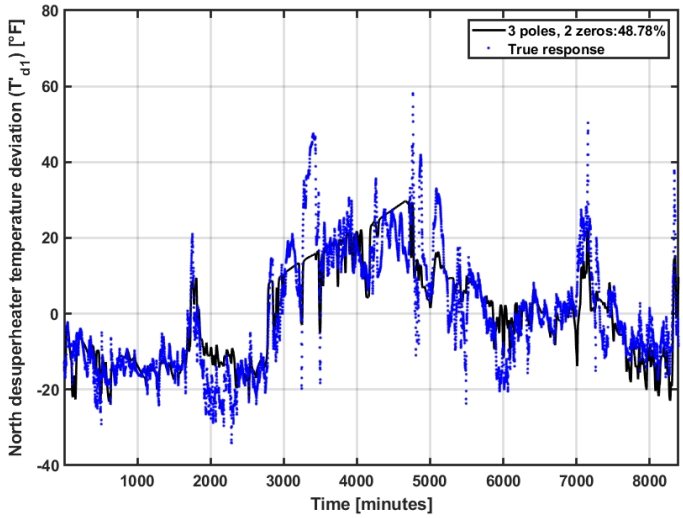

FIGURE 6: Three poles and three zeros transfer-function model validation for the north desuperheater over the entire dataset.

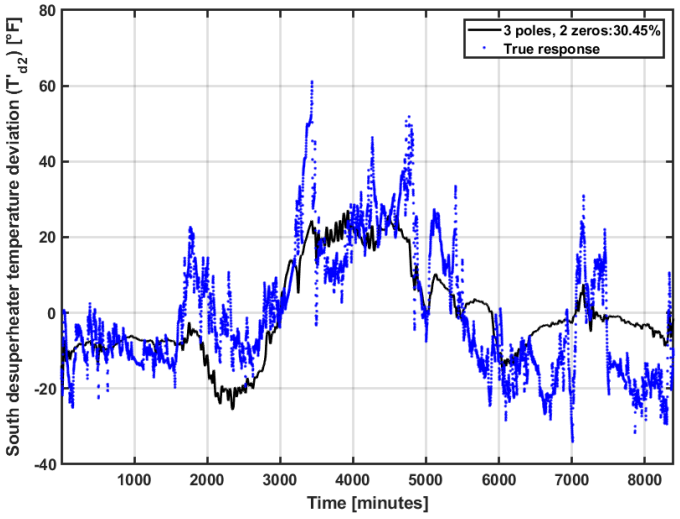

FIGURE 7: Three poles and two zeros transfer-function model validation for the south desuperheater over the entire dataset.

Next, the hypothesis of possible changes in the control states is investigated. The transfer function structures obtained for both north and south desuperheaters are fixed and used to predict the system behavior at different loads from the nominal, half ($242MW$), and low ($82MW$), as well as other load conditions similar to the nominal ($425MW$ and $426MW$). The TF coefficients obtained at these other load conditions are compared to the coefficients of the selected transfer functions evaluated from the structure selection shown in Figs. 4 and 5. The comparison is conducted by calculating the relative deviations between the coefficients of the transfer functions. The magnitude of the observed deviations indicates whether a possible control state change happens or not. All observed deviations in the coefficients for both north and south desuperheaters are shown in Figs. 8 and 9.

Regarding the deviations observed in the transfer function coefficients for the north desuperheater (Fig. 8), for loads similar to the nominal (Fig. 8a), the maximum deviation observed is approximately 600%, which in this work is considered a low deviation and insignificant to evidence a control state change. The observed low deviation is expected, considering that the loads are about the same as the nominal load used to define the fixed transfer function structure. Conversely, the deviations for the half and low load cases (Figs. 8b-c) are shown in general to be of higher order. The maximum deviation between the nominal state and the half load is approximately $21,000\%$, while between the nominal state and the low load is approximately $80,000\%$, both being considered as high deviation values. Lastly, when comparing the observed deviations shown in Figs. 8b-c between the half and low load, it is possible to see that they both have about the same order of magnitude. Overall, for the north desuperheater, it can be seen that there is a clear control state change when going from the nominal state to both the half and low loads, but not from the half to the low load. Therefore, to account for this, the re-tuning of the controller or the re-ranging of the control valve might be desirable when going from the nominal to the half and low loads, but it is not necessary when going from the half to the low load.

Now, considering the deviations of the transfer function coefficients for the south desuperheater (Fig. 9), the deviation observed from the nominal state to the half load (Fig. 9b) is of approximately $2,000\%$, while between the nominal state and the low load (Fig. 9c) is approximately $120,000\%$. In this case, it can be seen that there is a clear control state change when going from the nominal state to the low load but not from the nominal to the half load. Comparing the deviations observed for loads similar to the nominal (Fig. 9a), for most of the coefficients, deviations are of low order, not exceeding $1,000\%$, except for $b2$ where a deviation of $20,000\%$ is observed and treated as an outlier. Overall, based on the observed deviations for the south desuperheater, the re-tuning of the controller or the re-ranging of the control valve might be required when going from the nominal and half loads to the low load, but it might not be necessary when going from the nominal to the half load scenario.

It is also important to mention that the control state changes happened for both north and south desuperheaters but in different ways. For the north desuperheater, the control state changes are evidenced when going from the nominal to the half and low loads but not when going from the half to the low load. Meanwhile, control state changes are evidenced for the south desuperheater when going from the nominal to the low load but not from the nominal to the half load. Although the power plant owner of the data used in this work did not disclose any details on the

configuration of the desuperheaters, this difference in the control state change behavior is believed to exist as a result of differences between the heat exchange surface areas of each desuperheater caused by maintenance and repairs over the years.

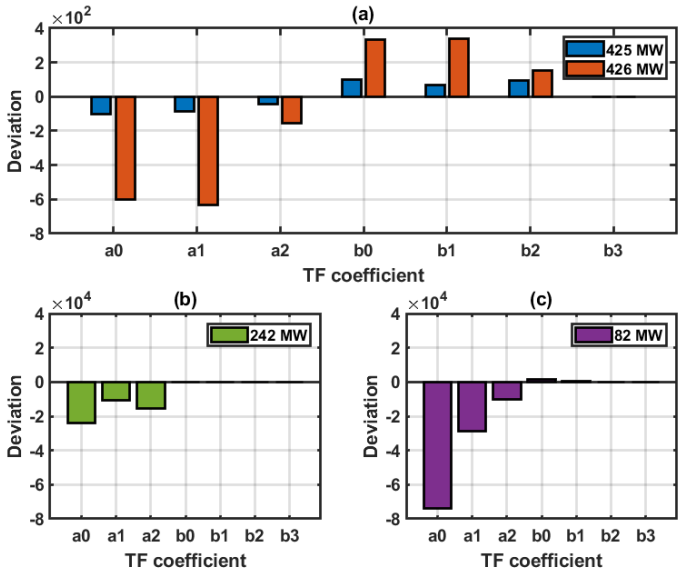

FIGURE 8: Transfer function coefficient comparisons for full, half, and low loads vs. nominal load for the north desuperheater.

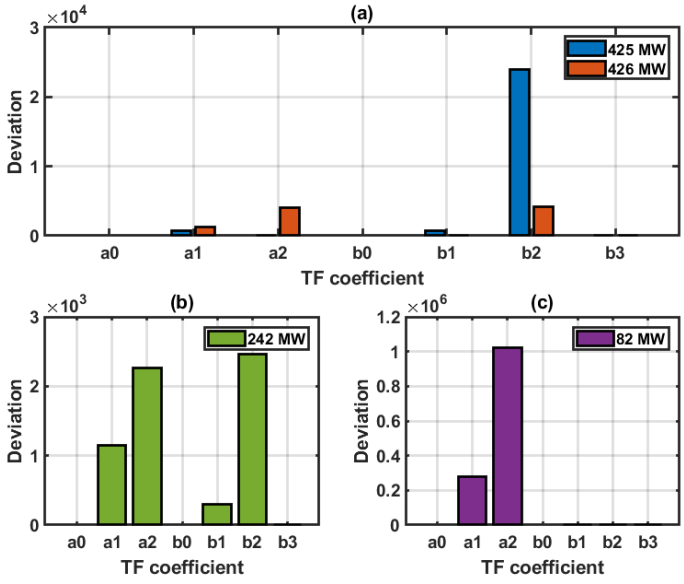

FIGURE 9: Transfer function coefficient comparisons for full, half, and low loads vs. nominal load for the south desuperheater.

4.2 System Identification with Nonlinear Auto-Regressive model structure with eXogenous inputs (GP-NARX)

The availability of high-performance machine learning tools, such as Gaussian Processes, and their particular ability to quantify uncertainty have motivated the second part of this study, in which GPs are applied to verify changes in the control states. Following the same approach as in section 4.1, initially, a single GP-NARX

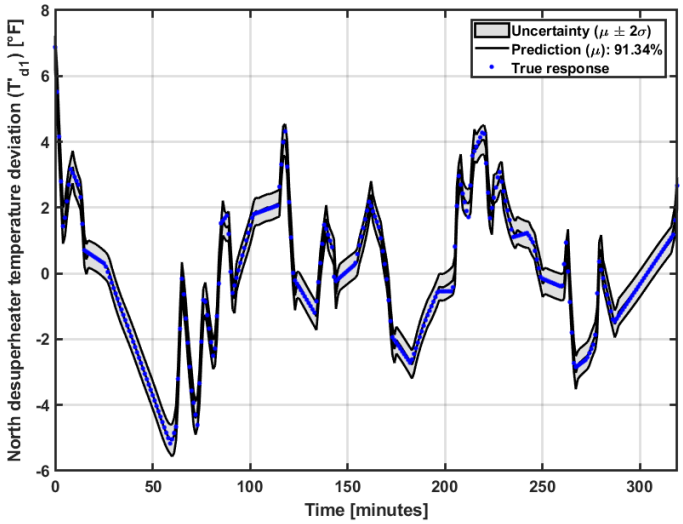

FIGURE 10: GP-NARX for the north desuperheater controlled variable with accuracy (GoF) and uncertainty shown.

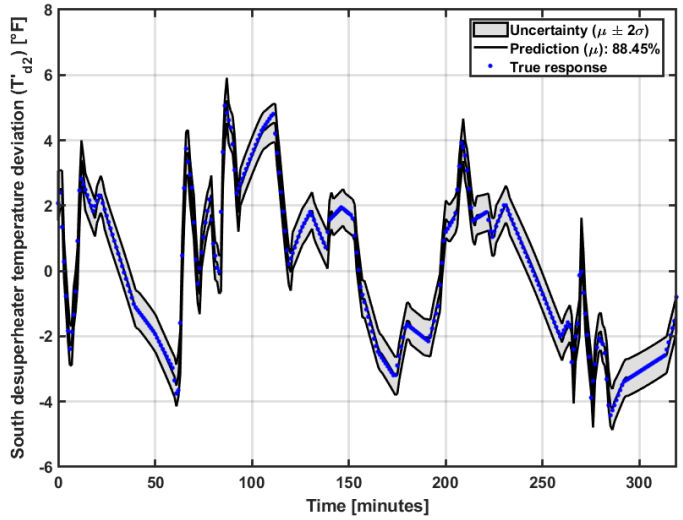

FIGURE 11: GP-NARX for the south desuperheater controlled variable with accuracy (GoF) and uncertainty shown.

to describe the input-output relationship for each desuperheater is identified, and its prediction capabilities are assessed. The same specific data sample with 322 points sampled each minute at the nominal state is selected as the training data. Given the structure of the GP-NARX model equations and discrete-time characteristics, input and output lags must be specified (both are set equal to 2). Before performing the identification, prior informed parameters are specified for the GP. The configuration set chosen can be found in Tab. 2. Figs. 10 and 11 display the model identification results, evidencing the capabilities of GP-NARX structures to predict not only the average value of the real data (μ) but also the uncertainty region ($\mu \pm 2\sigma$). The GP-NARX model describing the input-output relation for the north desuperheater is shown in Fig. 10. Prediction accuracy is again evaluated using the GoF with NRMSE as the cost function. It is possible to see that GP-NARX fits the true system behavior with an accuracy of 91.34%.

For the south desuperheater, the fit accuracy is 88.45%, as shown in Fig. 11. Both GP-NARX models presented are within the confidence bounds and exemplify how the GP has a higher accuracy in performing system identification when compared against traditional system identification techniques, such as the transfer function approach used in Section 4.1.

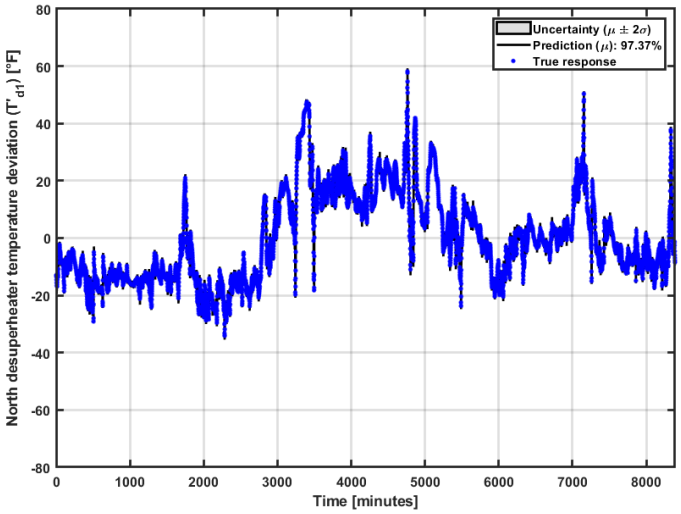

FIGURE 12: GP-NARX validation on identification data over the entire dataset for the north desuperheater with accuracy (GoF) and uncertainty shown.

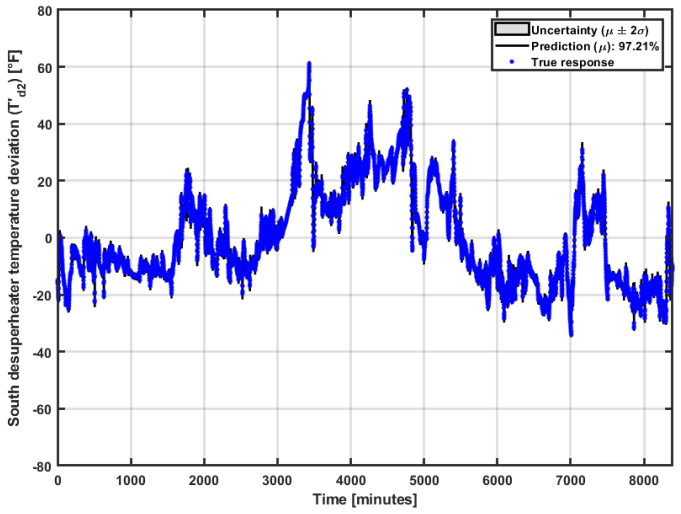

FIGURE 13: GP-NARX validation on identification data over the entire dataset for the south desuperheater with accuracy (GoF) and uncertainty shown.

Next, the validation of the GP-NARX structure obtained is performed considering the entire system behavior, similar to the validation of the selected transfer function structures shown in Figs. 6 and 7. For this step, the hyperparameters are re-optimized using the entire system data with 8,392 points. The obtained results for the validation of the GP-NARX are shown in Figs. 12 and 13. The plots again show the high accuracy capabilities of GP models when performing system identification. In Fig. 12, the accuracy in prediction for the north desuperheater is 97.37%, while for the south desuperheater, the prediction accuracy is 97.21%. The higher accuracy values shown for the validation of the entire system behavior are expected, considering that whenever more data is given for the training of the GP model, the prediction is usually more reliable. This latter result is another example of the enhanced features that GP potentially offers. However, it is also worth mentioning that whenever more data is given at the identification step, more time is required for training due to the computational complexity of the matrix inversion operations when handling the covariance matrix at the GP training step.

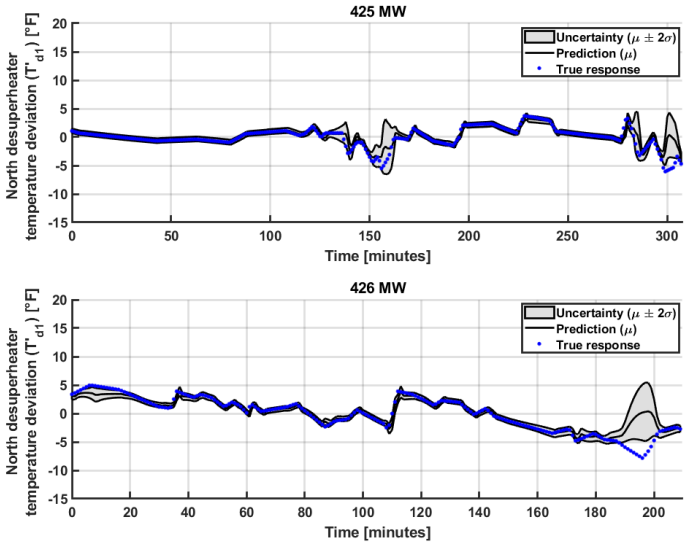

FIGURE 14: GP-NARX validation at different full loads for the north desuperheater.

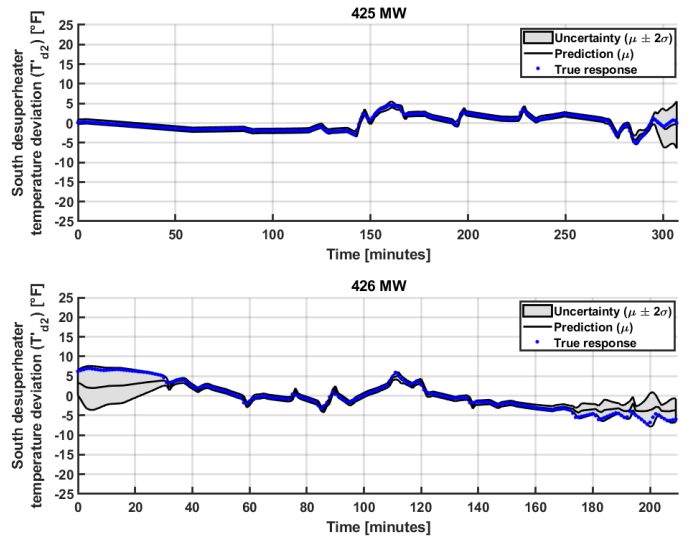

FIGURE 15: GP-NARX validation at different full loads for the south desuperheater

Considering similar ($425MW$ and $426MW$) and different operating load scenarios ($242MW$ and $82MW$), the GP-NARX models trained at the selected nominal state ($430MW$) for both

north and south desuperheaters are used to simulate these other load operating conditions. The premise is that under different system loads from the nominal, the uncertainty might enlarge due to a change in the control state, while for similar load operating conditions, the uncertainty is expected to shrink.

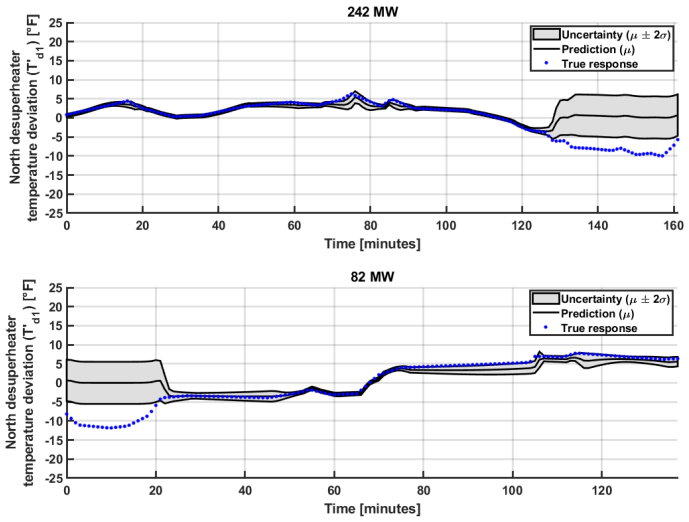

FIGURE 16: GP-NARX validation at both half and low loads for the north desuperheater.

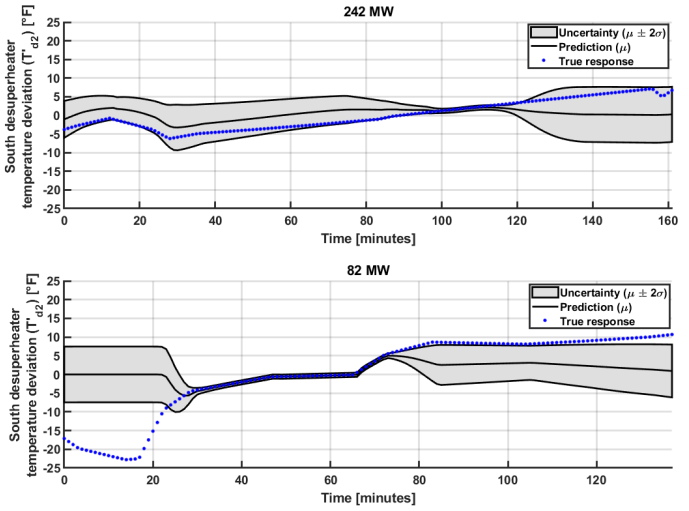

FIGURE 17: GP-NARX validation at both half and low loads for the south desuperheater.

Figs. 14 and 15 show the prediction and uncertainty obtained at operating loads similar to the nominal, for the north and south desuperheaters, respectively. One can see that the GP-NARX model has the prediction within the confidence bounds for most of the data with a few outliers. The system trends and predictions when operating at the half load ($242MW$) are exhibited in Figs. 16 and 17. It is possible to observe that for the north desuperheater, although most part of the data is within the confidence bounds, offset and increased uncertainty are observed in the last part of the data. Meanwhile, for the south desuperheater, an increased uncertainty is observed for most of the data, and a mismatch in the prediction occurred when compared to the true system behavior. Inspecting the system trends and predictions when operating at the low load ($82MW$) in Figs. 16 and 17, it is possible to see that for the north desuperheater, most part of the data points are within the confidence bounds, but offset and increased uncertainty are observed at the beginning. Meanwhile, for the south desuperheater, enlarged uncertainty and mismatch are observed for most of the data, with a substantial offset between the prediction and the true system behavior in the first 20 minutes.

If the half and the low load conditions are compared for the south desuperheater, it is possible to see that the uncertainty and the offset for the GP-NARX predictions increase significantly. This evidences a considerable change in the control state when transitioning from the nominal to the low load conditions, while for the half load, although the observed uncertainty is also enlarged, the offset is not as significant as it is for the low load. These latter observed results align according to what was seen using the transfer function approach. Hence, for the south desuperheater, the re-tuning of the controller or the re-ranging of the control valve might be required when going from the nominal and half loads to the low load, but it might not be necessary when going from nominal to the half load. Regarding the north desuperheater, increased uncertainty and mismatches are only observed at the beginning and the end in Fig. 16. However, these observed mismatches are more significant in extension than the ones observed when comparing loads similar to the nominal load. Therefore, although not as strong as evidenced in the south desuperheater, these observed uncertainties can also be exploited in a control algorithm to inspect the maximum allowable variance or standard deviation of the GP-NARX structure as a trigger for re-tuning controllers when operating at different loads.

5. CONCLUSIONS

This work investigated the identification of possible control state changes in a power plant system composed of two desuperheaters (i.e., north and south) using real closed-loop data from a coal-fired power plant operated nominally at $430MW$. For the transfer function approach, three poles and two zeros transfer functions were used to identify distinct control states for the desuperheaters. The control states of the north desuperheater shifted when changed from the nominal to the half and low loads. Regarding the south desuperheater, changes in the control states were observed when going from the nominal state to the low load but not from the nominal to the half load. Control state characterization using the GP-NARX scheme generated a consistent result with the TF analysis, particularly for the south desuperheater, in which a significant uncertainty and mismatch in prediction evidenced a change in the control state from the nominal to the low load, while for the half load, it was not as significant as it was for the low load. Regarding the north desuperheater, although increased uncertainty and mismatches were observed at shorter time intervals when compared to the south desuperheater, they were more significant in extension than the ones observed when comparing loads similar to the nominal load. Therefore, this work shows that both approaches can be used to identify the control state changes using closed-loop data from real coal power plants. In future work, the approaches developed in this study can be used

as a basis for online system identification, employing real power plant data. Moreover, a control algorithm could be developed to inspect the maximum coefficient deviation in the TF approach or maximum allowable variance in the GP-NARX approach as possible triggers for re-tuning controllers when operating at different loads.

ACKNOWLEDGMENTS

This work was supported by the Advanced Sensors, Controls, and Novel Concepts Program, Office of Fossil Energy and Carbon Management. The authors also thank the National Science Foundation RII Track-2 FEC (OIA-2119688) and West Virginia University for additional support.

DISCLAIMER

REFERENCES

[1] Agbleze, Selorme, Lima, Fernando V., Indrawan, Natarianto, Panday, Rupendranath, Pezzini, Paolo, Bonilla-Alvarado, Harry, Bryden, Kenneth M., Tucker, David and Shadle, Lawrence J. "Modeling and Control of Subcritical Coal-Fired Power Plant Components for Fault Detection." *ASME 2020 Power Conference*. 2020. DOI 10.1115/POWER2020-16571.

[2] Agbleze, Selorme, Shadle, Lawrence J. and Lima, Fernando V. "Dynamic Modeling and Simulation of a Subcritical Coal-Fired Power Plant Under Load-Following Conditions." *Industrial and Engineering Chemistry Research.* (2024)DOI 10.1021/acs.iecr.4c00494.

[3] Cho, Baekhyun, Choi, Geunwon, Uruno, Yumi, Kim, Hyunseo, Chung, Jaewon, Kim, Hyojun and Lee, Kihyun. "One-dimensional simulation for attemperator based on commissioning data of coal-fired steam power plant." *Applied Thermal Engineering* Vol. 113 (2017): pp. 508–518. DOI 10.1016/j.applthermaleng.2016.11.069.

[4] Kim, Rebecca and Lima, Fernando V. "Nonlinear multi-objective and dynamic real-time predictive optimization for optimal operation of baseload power plants under variable renewable energy." *Optim Control Appl Methods* Vol. 44 No. 2 (2023): pp. 798–829. DOI 10.1002/oca.2852.

[5] Forssell, Urban and Ljung, Lennart. "Closed-loop identification revisited." *Automatica* Vol. 35 No. 7 (1999): pp. 1215–1241. DOI 10.1016/S0005-1098(99)00022-9.

[6] Wang, Di, Wu, Xiao and Shen, Jiong. "An Efficient Robust Predictive Control of Main Steam Temperature of Coal-Fired Power Plant." *Energies* Vol. 13 No. 15 (2020): p. 3775. DOI 10.3390/en13153775.

[7] Ljung, Lennart. *System Identification Theory for the User*, 2nd ed. Pearson Education, Limited, Sydney (1998).

[8] LeBlanc, Steven E. and Coughanowr, Donald R. *Process systems analysis and control*, 3rd ed. McGraw-Hill Higher Education, Boston (2009).

[9] Seborg, Dale E. *Process dynamics and control*, 3rd ed. John Wiley & Sons, Inc, Hoboken, N.J (2011).

[10] Karimi, Kamran and Hamilton, Howard J. "Generation and Interpretation of Temporal Decision Rules." (2010). ArXiv:1004.3334 [cs].

[11] Sjöberg, Jonas, Zhang, Qinghua, Ljung, Lennart, Benveniste, Albert, Delyon, Bernard, Glorennec, Pierre-Yves, Hjalmarsson, Håkan and Juditsky, Anatoli. "Nonlinear black-box modeling in system identification: a unified overview." *Automatica* Vol. 31 (1995): pp. 1691–1724. DOI 10.1016/0005-1098(95)00120-8.

[12] Rasmussen, Carl Edward and Williams, Christopher K. I. *Gaussian Processes for Machine Learning*. The MIT Press (2005). DOI 10.7551/mitpress/3206.001.0001.

[13] Kocijan, Juš. *Modelling and Control of Dynamic Systems Using Gaussian Process Models*. Springer International Publishing (2016). DOI 10.1007/978-3-319-21021-6.

[14] Forrester, Alexander I. J., Sóbester, András and Keane, A. J. *Engineering design via surrogate modelling: a practical guide*. J. Wiley (2008).

[15] Paniagua, Jose L. and López, Jesús A. "Nonlinear system identification using modified variational autoencoders." *Intelligent Systems with Applications* Vol. 22 (2024). DOI 10.1016/j.iswa.2024.200344.

